ISSN No. 2278-2540 | DOI: 10.51583/IJLTEMAS | Volume XV Issue XI November 2026

Compressed Air Motor with Ratchet-Type Coupling Mechanism

Alfred Rufer

STI-DO, EPFL, Swiss Federal Institute of Technology Lausanne, Switzerland

DOI : https://doi.org/10.51583/IJLTEMAS.2026.151100042

Received: 07 November 2026; Accepted: 12 November 2026; Published: 25 November 2026

ABSTRACT

An unconventional compressed-air engine is presented which is composed of a specific pneumatic cylinder assembly of high efficiency and of a special coupling mechanism using lever arms driving ratchet-type or clutch bearings for the transformation of the linear motion of the actuator into the rotation of the engine shaft.

More precisely this study investigates the possibility to vary the generated torque through variation of the length of the lever arms and through the introduction of multiple interventions of the actuator during one revolution of the engine. The form of the produced forces and of the generated torque contributions are simulated according to a dedicated kinematic model. The study is completed by an estimation of the energetic efficiency and a small demonstrator has been realized.

INTRODUCTION

Compressed air engines have been proposed in many contexts of use and in many different technologies. Their main advantages are in the simplicity and reliability of the technology, and in the acquisition costs of the equipments. Near standard industry applications in production of goods, handling or moving of objects, another application field in the energy sector concerns compressed air energy storage where conversion engines are used. Compressors are filling the storage reservoirs while in the recovery path expansion turbines or motors are placed between the storage vessel itself and the electrical generation machine (1-4). The classical compressed air machines go from rotary vane type to piston/crankshaft types, through gear type or turbine type motors. In general, these motors have a low energetic efficiency due to their principle of conversion where only displacement work is produced in the machine (5-7). Recent developments in the field of pneumatic to mechanical conversion allow to strongly increase the energetic performances of such machines. These benefits are realised through the addition to the conversion principle of a second torque component resulting from a real thermodynamic expansion inside of the active volume or in an added supplementary chamber of larger dimensions (8-11).

Pneumatic drives for propulsion of vehicles have also been proposed with very different energetic performances. Transformed machines initially running with internal combustion of fuel have been proposed as zero-emissions vehicles, also dedicated architectures with increased efficiency (12-15).

Previous work has described an original compressed air engine where the conversion of the compressed air energy is realized on the base of so-called PAMs, Pneumatic Artificial Muscles (16-18). After the study of a system based on a classical crankshaft, an original architecture has been proposed where the artificial muscles are driving the shaft of the engine with lever-arms which impose their sectorial rotation through freewheel clutch bearings (19-20).

In a further study, the coupling mechanism has been transformed into a specific mechanism allowing the coupling of both the pulling and the pushing effort of the actuator into a rotational movement (21).

This mechanism is re-used in the present studied engine. Instead of using a PAM as a primary actuator, the present engine uses classical linear piston-cylinders in an original assembly allowing to reach an increased

ISSN No. 2278-2540 | DOI: 10.51583/IJLTEMAS | Volume XV Issue XI November 2026

energy efficiency (22, 11). A first description of the original architecture has been given in (23) where the system has been simulated and a small demonstrator has been presented. In the present paper, the same architecture is studied again, but with a specific accent on the capability of increasing the mechanical torque by variation of the length of the lever-arms, and with multiple interventions of the pneumatic actuator within one revolution of the engine's shaft. Figure 1 illustrates the concept of the new engine.

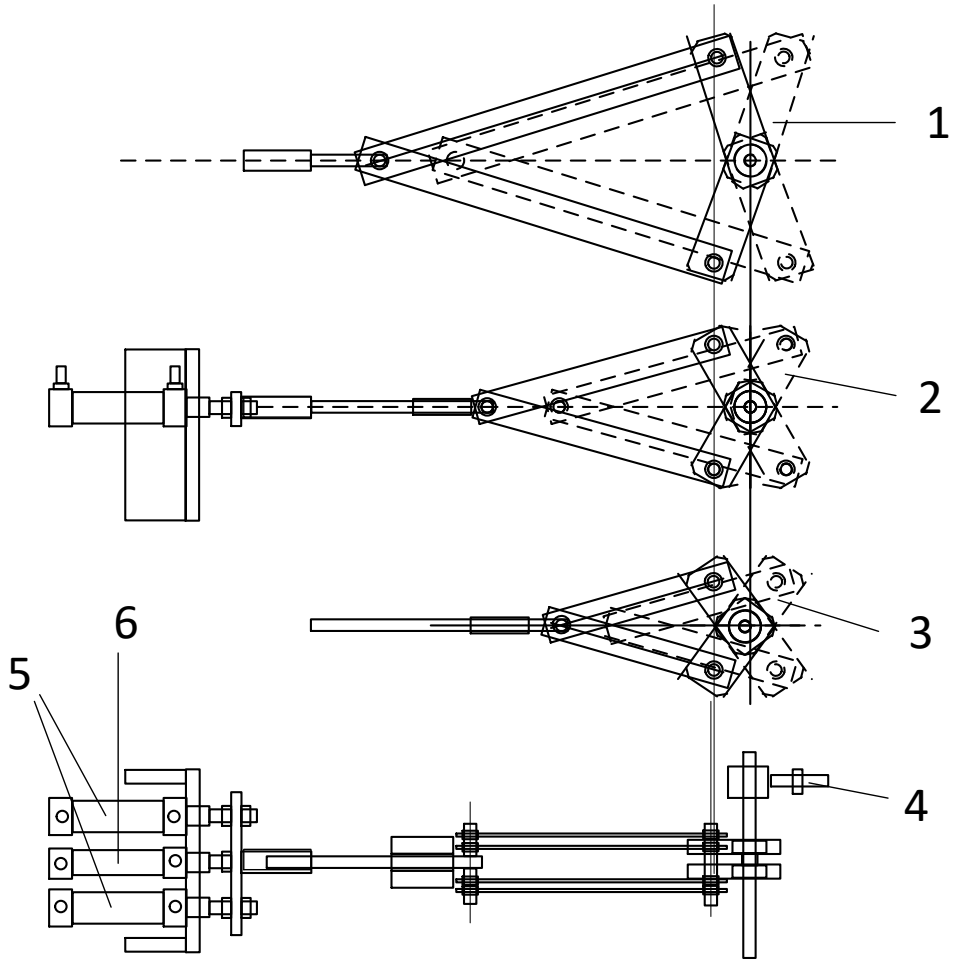


Figure 1 Architecture of the proposed engine with the different dimensions of the coupling mechanism.

Description of the System

Three versions of the new system are illustrated in Fig. 1 with three different lengths of the lever-arms driving the engine shaft through freewheeling clutch bearings. On the left central and lower left part of the figure, the pneumatic actuator can be seen. The original assembly of this actuator is based on the principle of combining displacement work and thermodynamic expansion. This principle uses a central bidirectional cylinder where the filling of the chambers is done with air at constant pressure (part 6 in Fig. 1). Then, during the following return stroke, the air is expanded by a transfer from the central cylinder into the chambers of two lateral cylinders running in parallel (parts 5 in Fig. 1).

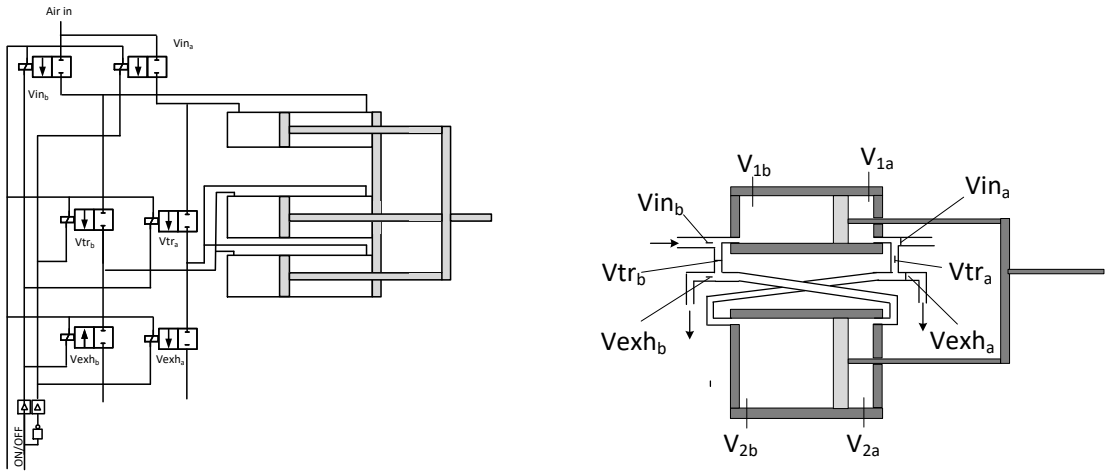
On the right side of the figure three different variants of the coupling are represented. Corresponding to the originally described system (ref. 23) the central illustration shows a solution where the length of the lever-arms is equal to the stroke of the actuator (50mm), (part 2 in Fig. 1) The upper system has an increased length of the levers of 50%, namely 75mm (part 1 in Fig. 1).

The lower system has 35mm length of the levers (part 3 in Fig. 1). The motion of the actuator is transmitted to the lever-arms with connecting rods. For all three systems the ratio of the length of the connecting rod to the length of the lever-arms is identic (connecting rod ratio λ).

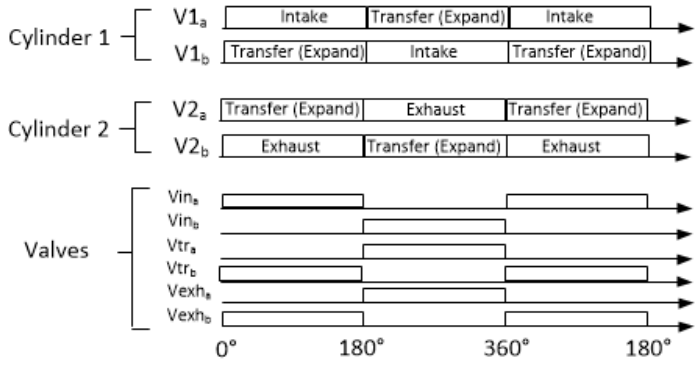
ISSN No. 2278-2540 | DOI: 10.51583/IJLTEMAS | Volume XV Issue XI November 2026

A cylinder assembly for an actuator with higher efficiency

The principle of recovering the thermodynamic content of the pressurized air is applied to linear cylinders, where in addition to the simple displacement work usually produced in a conventional cylinder, the air is additionally expanded in a supplementary pneumatic chamber system, allowing to recover a significant part of the injected enthalpy [11].



a) b)



c)

Figure 2 Principle of operation a) cylinder arrangement with control valves, b) equivalent of volumes, c) Control diagram

Operating principle and control

The pneumatic actuator of the present engine is an assembly of individual cylinders as represented in Fig. 1 and 2a. The chambers of the central cylinder are fed from the air reservoir under constant pressure. Then the air is transferred into the chambers of the two other cylinders running in parallel.

As represented in the diagram of Fig. 2a, two intake valves Vin_a and Vin_b are feeding alternately the pulling and pushing chambers of the first cylinder. The transfer of the air from the first cylinder to the two others is controlled through the two transfer valves Vtr_a and Vtr_b. Finally, after the expansion, the air at the final expansion pressure is released to the external atmosphere through two exhaust valves $Vexh_a$, $Vexh_b$. The sequences of operation are defined according to the diagram of Fig. 2c.

The simulation of the system is considering a simplified model where the two parallel running cylinders are represented by one cylinder of the corresponding larger volume (Fig. 2b). In the studied example, a central

ISSN No. 2278-2540 | DOI: 10.51583/IJLTEMAS | Volume XV Issue XI November 2026

cylinder of 12mm diameter is chosen with two lateral ones of each 16mm diameter. As a result, the volumetric ration for expansion is of 3.55.

The pressure variation during expansion

The expansion of the air is supposed to be of the adiabatic type. This assumption is based on the fact that the air flows rapidly and does not rest in the cylinders, with the consequence that the thermal transfer time is too short. The resulting pressure P_2 in the chambers V_{2a} (first half-cycle) and V_{2b} (second half-cycle) and of the feeding chambers V_{1b} and respectively V_{1a} takes the value of

$$P_2 = P_{in}\left(\frac{V_{1\max}}{V_{1a,b}+V_{2b,a}}\right)^{\gamma} \quad \text{with } \gamma = 1.4 \qquad (1)$$

P_2, V_{1a}, V_{2b} respectively $P_{2'}$, V_{1b}, V_{2a} are system variables which change during the expansion phases in dependency of the piston's displacement during the first, respectively the second half period. For example, V_{1a} is decreasing during the "push" stroke, while V_{2b} is increasing.

With the dimensions of the chosen cylinders of respectively 12 and 16 mm, the ideal volume ratio which appears at the end of the stroke becomes

$$\frac{V_i}{V_f} = \frac{l\cdot\pi D_1^{\,2}/4}{2\cdot l\cdot\pi D_2^{\,2}/4} = \frac{0.012^2}{2\cdot 0.016^2} = 0.281 \qquad (2)$$

V_i corresponds to the initial (maximum) value of the chambers of the central cylinder, and V_f corresponds to the final value of the sum of the feeding and of the expanding chambers of the two parallel running lateral ones. The corresponding final pressure ratio becomes

P_2/P_{in}= 0.169 according to rel. (1).

In the real case, there is an asymmetry of expansions and forces between the right- and the left side of the pistons in the cylinders. The asymmetry is due to the presence of the piston rod inside of one of the cylinder chambers (at the pushing side) which reduces the pressure area. Table 1 shows the values of the parameters of the chosen cylinders, their active surfaces in the push and pull motions, together with the length of the strokes.

Cylinder type	Bore size	Pressure area (push)	Pressure area (pull)	Stroke
MI12-50	12 mm	113 mm^2	93.4 mm^2	50 mm
MI16-50	16 mm	201 mm^2	181 mm^2	50 mm

Table 1 Parameters of the cylinders

The asymmetry of the pressure areas affects first the produced force caused by a given pressure, and second, it causes an asymmetry of the volumes, which further have their effect on the expansion ratio in the push and pull modes. The volume $V_{1a\max}$ at the pull side (right side) of the 12 mm cylinder is

$$V_{1a\max} = l\cdot\pi(D_1^{\,2} - d_{rod}^2/4 = 0.050\cdot\pi\cdot(0.012^2 - 0.006^2)/4 = 4.24\cdot 10^{-6} m^3 \qquad (3)$$

d_{rod} being the diameter of the piston rod (Figure 3)

ISSN No. 2278-2540 | DOI: 10.51583/IJLTEMAS | Volume XV Issue XI November 2026

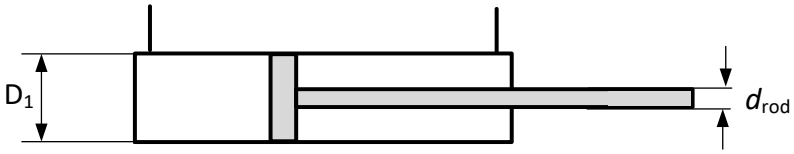


Figure 3 Diameters of cylinder and piston rod

At the push side (left side) V_{1bmax} is

$$V_{1b\max} = l \cdot \pi D_1^2 / 4 = 0.050 \cdot \pi \cdot (0.012^2) / 4 = 5.65 \cdot 10^{-6} m^3 \quad (4)$$

For the 16 mm cylinder, the volumes are respectively V_{2amax} and V_{2bmax}

$$V_{2a\max} = l \cdot \pi (D_2^2 - \mathrm{d}_{rod}^2 / 4 = 0.050 \cdot \pi \cdot (0.016^2 - 0.006^2) / 4 = 8.63 \cdot 10^{-6} m^3 \quad (5)$$

$$V_{2b\max} = l \cdot \pi D_1^2 / 4 = 0.050 \cdot \pi \cdot (0.016^2) / 4 = 10.05 \cdot 10^{-6} m^3 \quad (6)$$

Consequently, the volume and pressure ratios become

$$\frac{V_{1a\max}}{2 \cdot V_{2b\max}} = \frac{4.24 \cdot 10^{-6}}{2 \cdot 10.05 \cdot 10^{-6}} = 0.210 \quad (7)$$

$$\frac{P_{21}}{P_{in}} = \left(\frac{V_{1a\max}}{2 \cdot V_{2b\max}} \right)^{1.4} = 0.114 \quad (8)$$

$$\frac{V_{1b\max}}{2 \cdot V_{2a\max}} = \frac{5.65 \cdot 10^{-6}}{2 \cdot 8.63 \cdot 10^{-6}} = 0.327 \quad (9)$$

$$\frac{P_{22}}{P_{in}} = \left(\frac{V_{1b\max}}{2 \cdot V_{2a\max}} \right)^{1.4} = 0.2094 \quad (10)$$

Modeling of the Complete Engine

The produced mechanical work by the proposed system must be evaluated first as the effort produced by the cylinder assembly and then as the torque transmitted to the engine's shaft. The actuator assembly produces pulling and pushing forces, as contributions of four main components namely the forces generated by the intake pressure on the surfaces of the first piston and the forces generated by the expansion and exhaust pressures on the surfaces of the first and second one. Additionally, the four force components must be evaluated for the pull and push motion of the actuator. An analytic calculation of the sum of these eight components is not realistic, due to the fact that the expansion pressure depends on the position of the pistons which is imposed by the coupling mechanism and the angular position of the engine's shaft. Thus, the different variables are calculated by simulation of the complete system.

Structure of the coupling

For the representation of the variables of the complete system, a mathematic description of the kinematics of the coupling of the cylinder's piston rods to the engine's shaft is needed. Figure 1 has given a first view of the coupling mechanism which uses short lever-arms driving freewheeling clutch bearings. The end connection of the three pistons is maintained in line by a horizontal linear guide and is coupled to two connecting rods (Figures 1 and 4). The positive force of the cylinder assembly (acting from the right to the

ISSN No. 2278-2540 | DOI: 10.51583/IJLTEMAS | Volume XV Issue XI November 2026

left in Figure 4) is pulling the upper lever-arm and produces through the clutched bearing a torque which acts anticlockwise on the engine shaft. The clutch bearing of the lower lever-arm is freewheeling during this stroke. The negative force of the cylinder assembly (acting from the left to the right in Figure 4) is pushing the lower lever-arm and acts on the shaft with a torque in the same direction as the upper one during the previous stroke. The clutch bearing of the upper lever-arm is freewheeling during this stroke. The positive and negative actions of the cylinder assembly are defined over a limited angle (limited oscillating angle of the lever-arms), and distributed symmetrically on either side of a line perpendicular to the movement of the pistons, which passes through the shaft's point of rotation (see Fig. 4). In the present application, the active rotation angle φ_{act} is a result of the defined cylinder stroke Δl and the radius of gyration of the lever-arms r: $\varphi_{act}=2\cdot\text{asin}(\Delta l/2r)$ as represented in Figure 4.

For the radius of gyration of the lever-arms, r, three different values are chosen in order to evaluate its effect on the produced torque. In the first study (see ref. 23) r was chosen equal to the cylinder stroke Dl, resulting into an oscillation angle φ_{act} of 60°. In the present study there are three considered values of the ratio $r/\Delta l$ which are respectively 1.5, 1, and 0.7. (Table 2).

$r/\Delta l$	r [mm]	φ_{act} [°]	λ	l_{cr}
1.5	75mm	38.9°	3.28	246mm
1	50mm	60°	3.28	164mm
0.7	35mm	91°	3.28	114mm

Table 2 Parameters and oscillation angle of the lever-arms

From the simulation curves of the forces and of the torque (see next sections) and for the specific case of r=35mm, one can see the dead zone existing in the torque transmission when one intervention in each half period is controlled. This intermittency can be corrected with multiple interventions triggered from an adapted angular position sensor (see Figure 5). From Table 2 and with the values of φ_{act}, related to r=50 and 75mm, one can deduce that six interventions of the actuator during one revolution of the shaft can be triggered, namely three pushes and three pulls.

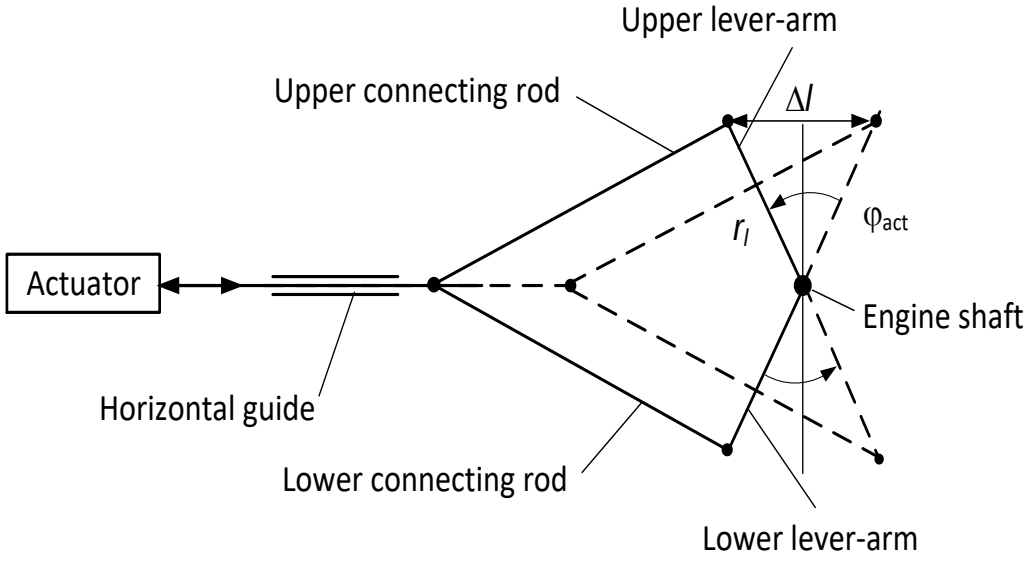


Figure 4 Scheme of the coupling mechanism

ISSN No. 2278-2540 | DOI: 10.51583/IJLTEMAS | Volume XV Issue XI November 2026

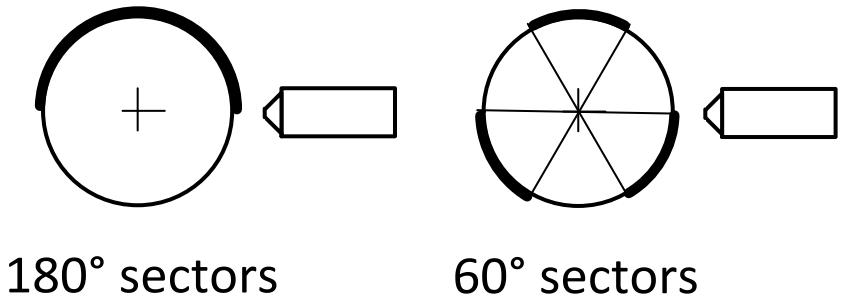


Fig. 5 Different sectors for the position sensor for the multiple torque interventions.

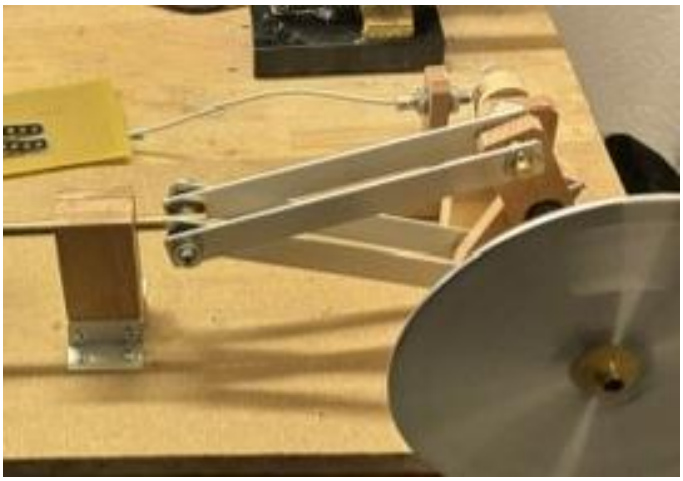


Figure 6 Detail view of the coupling (experimental set-up)

Simulation of the System

The simulation of the system is realized with a tool where the different elements are represented as functional blocks (Simulink). One period of rotation of the engine is simulated as a quasi-stationary phenomenon, and with an imposed value of the angular velocity (ω=6.28 rad/s).

An overview diagram of the implemented simulation is given in Fig. 7. From an angular position ωt, the different torque contributions in the pull and push strokes are calculated in the different sectors where the pneumatic actuator intervenes.

For each sector, a reference angle $\varphi_0+n*2\pi/n$ places the intervention within the engine's period. First, a geometric/trigonometric calculation gives the position x of the pistons from the angular position of the shaft (Block Nr. 1 in Fig. 7). The position x is calculated with the help of rel. 11. Depending on the position of the pistons, the active volumes on both sides of them are calculated (Block 2 in Fig. 7). Then with the variations of the volumes the expansion pressures (adiabatic expansions) are evaluated for the push and pull strokes of the actuator (Block 3 in Fig. 7). These pressures, together with the feeding pressure P_{in} and the exhaust (atmospheric) pressure P_{atm} determine the force components of the two sides of the pistons (Block 4 in Fig. 7). The block Nr. 5 calculates the total transmitted force of the actuator F_p , the force transmitted through the connecting rods F_s, and the resultant tangential force F_t responsible for the transmitted torque component M_n. The expressions for the different forces are given through rel. 14-16 in the next section, their physical meaning can be shown on the diagram of Fig. 8.

At the output, the different torque contributions M_n are added together to form the global torque M_{tot}. Finally, the value of the torque is multiplied by the angular velocity ω for the calculation of the mechanical power. The time-integral of the power (Block 7, 1/s in the figure) gives the value of the produced mechanical work.

ISSN No. 2278-2540 | DOI: 10.51583/IJLTEMAS | Volume XV Issue XI November 2026

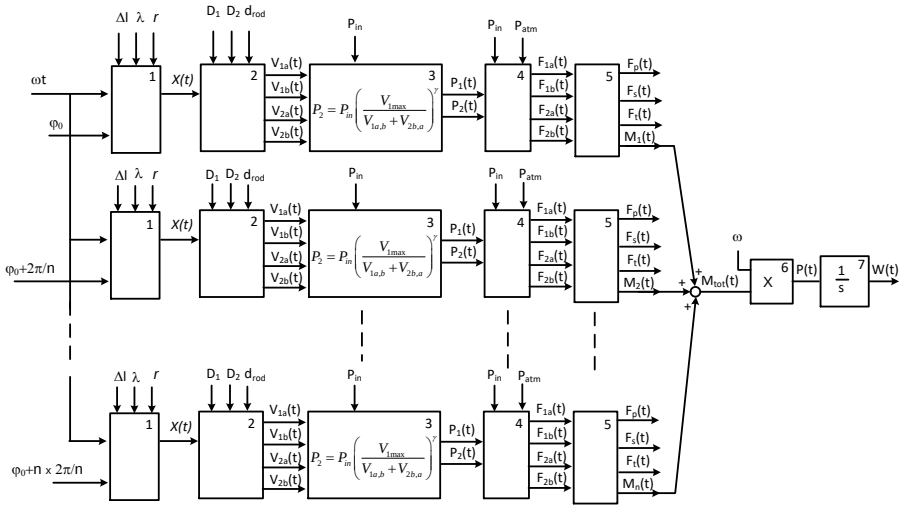


Fig. 7 Structural diagram for the implementation of the simulation of the engine.

Mathematical description of the lever-arm assembly

In Figure 8 the coupled cylinder assembly is represented with a connecting rod and a crankshaft used for the illustration of the lever-arm principle. The parameters are indicated as r_l, the radius of gyration of the lever-arm, l_{cr} the length of the connecting rod, and φ the angle of rotation of the crankshaft. The position of the end of the piston rod x is also indicated.

The relation between the position x of the actuator end and the rotation angle of the shaft is given through Rel. (11). This relation is valid for the status of the engaged clutch bearings.

$$x = r_l(1-\cos\varphi)+\frac{\lambda}{2}r_l\sin^2\varphi \qquad (11)$$

where the connecting rod ratio λ is used and is defined as

$$\lambda = \frac{r_l}{l_{cr}} \qquad (12)$$

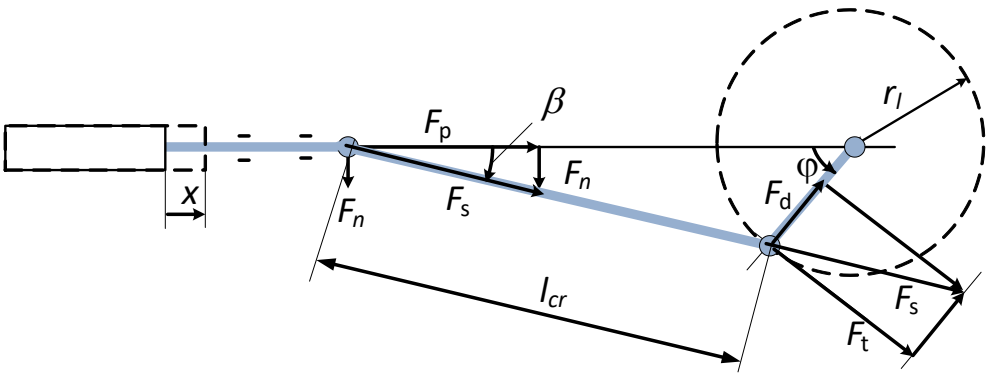


Figure 8 Diagram of the forces for the calculation of the torque and of the reactions

The torque on the crankshaft is given by Rel.13.

$$M_{mot} = F_t \cdot r_l \qquad (13)$$

With the tangential force F_t which is given by (14)

ISSN No. 2278-2540 | DOI: 10.51583/IJLTEMAS | Volume XV Issue XI November 2026

$$F_t = F_s \cos(\pi/2 - (\beta + \varphi)) \quad (14)$$

The force transmitted through the connecting rod F_s is calculated from the actuator's force F_p and the angle beta (15)

$$F_s = \frac{F_p}{\cos\beta} \quad (15)$$

This angle is given by Rel. (16)

$$\beta = arc\sin\left(\frac{r_l}{l_{cr}} \cdot \sin\varphi\right) \quad (16)$$

The power produced at the shaft level is also defined

$$P_{mech} = M_{mot} \cdot \omega \quad (17)$$

Simulation results

Figure 9 illustrates the behaviour of the system for the three cases where r is equal to 35, 50 and 75 mm respectively. In the first line of the figure, the forces inside and exerted by the cyllinder assembly are represented (Fig. 9 a), d), and g). The blue curves show the contributions of the cylinder Nr.1. It is the result of the contribution of the intake side (constant pressure) and of the expansion side of the piston. At the beginning of the strokes, after the opening of the transfer valve, the pressures in both chambers of the cylinder are identic if the dead volumes are neglected. The presence of a dead volume (related to the tubing and to the internal volume of the valve) causes in the real case a kind of pre-expansion. But the produced forces are different due to the assymmetric active surfaces of the piston. The force caused by the constant intake pressur minus the force caused by the decreasing expansion pressure results into the represented increasing form (blue curves). The red curves represent the contributions of the two lateral cylinders (represented by the cylinder Nr. 2 in the equivalent scheme of Fig. 2b) where one side receives the variable expansion pressure and where the opposite side is in the exhaust mode (atmospheric pressure). The yellow curves give the form of the global forces of the actuator.

The second line of the figure (Fig. 9 b), e), and h) illustrates the form of the lever forces, namely the actuator force F_p (blue), the force transmitted by the connecting rods F_s (red), and finally the tangential force F_t (yellow).

One can see the alternating values of the different forces related to the asymmetry of the surfaces of the pistons between their push and pull sides (presence of the piston rod in one chamber (push side).

The third line of the figure (Fig. 9, c), f) and i)) shows the form of the produced torques.

Figure 10 shows in its first line (Fig. 10, a), c) and e) the mechanical power transmitted. Finally, the second line of Fig. 10 shows the mechanical work produced by the engine (Fig. 10, b), d), and f)).

For a value of r of 35mm (Fig. 9 a), b), c), and Fig. 10 a) and b) the intervention of the actuator is triggered two times in one revolution of the engine (one push and one pull). The control signal is generated by a sensor with a 180° active sector (Fig. 5). The value of j_{act} of 91° does not allow more interventions.

For the case with r=50mm the resulting angle φ_{act} is equal to 60°. With an appropriate sensor with three active sectors of 60°, the interventions can be juxtaposed (Fig. 9 d), e), f) and Fig. 10 c), and d)).

For the case with r=75mm where the angle φ_{act} is of 38,9°, the same sensor with 60° resolution is used. The consequence is that the resulting torque becomes intermittent (Fig. 9 g), h), and i) and Fig. 10 e), and f)).

ISSN No. 2278-2540 | DOI: 10.51583/IJLTEMAS | Volume XV Issue XI November 2026

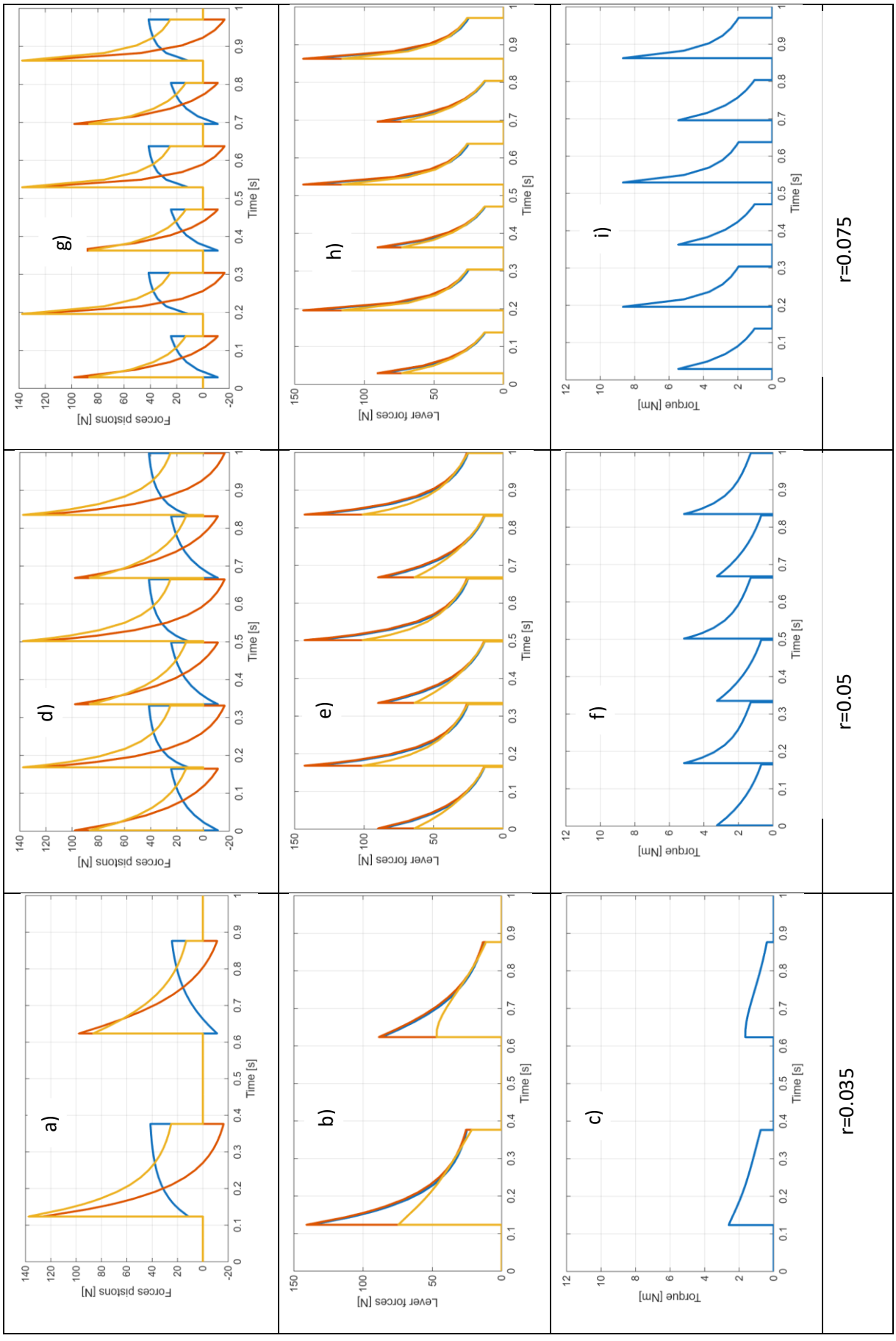


Figure 9 Simulation curves

ISSN No. 2278-2540 | DOI: 10.51583/IJLTEMAS | Volume XV Issue XI November 2026

r=0.035, a) Piston forces, blue : cylinder 1, red: cylinder 2, yellow: actuator force, b) Lever forces, red:actuator force F_p, blue: force of the connecting rod F_s, yellow: tangential force F_t , c)Torque

r=0.05, d), e),f), Idem a), b), c); r=0.75, g), h), i), Idem a), b), c)

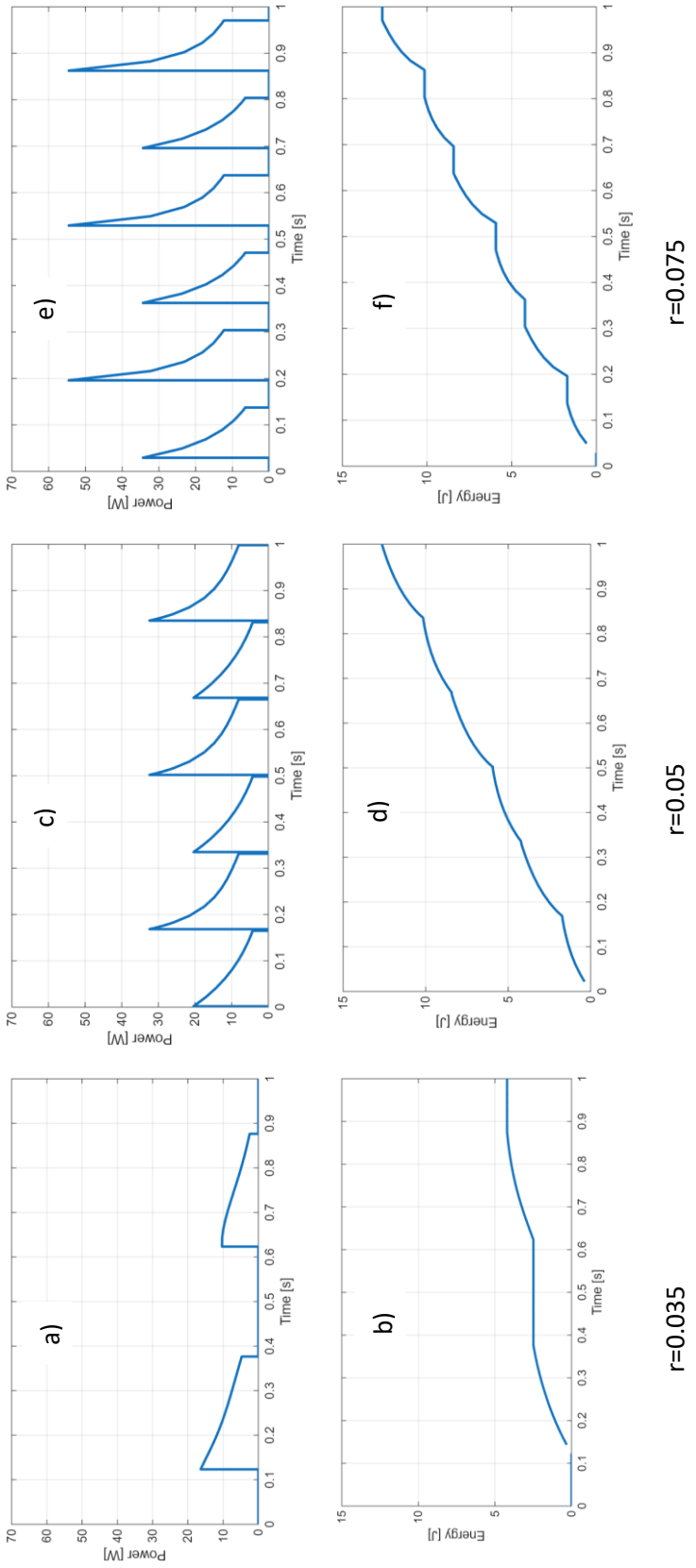


Figure 10 Simulation curves

ISSN No. 2278-2540 | DOI: 10.51583/IJLTEMAS | Volume XV Issue XI November 2026

r=0.035, a)Powe, b) Converted energy

r=0.05, c), d), Idem a), b), r=0.075, e), f), Idem a), b)

Energy Efficiency

To evaluate the energy efficiency of an air engine, the ratio of the mechanical work produced, W_{out} , to the enthalpy, H_{in} , of the injected air is calculated (Rel. 18).

$$\eta_{conv} = \frac{W_{out}}{H_{in}} \quad (18)$$

The value of the produced mechanical work W_{out} is obtained in the simulation from the integration of the instantaneous power P_{mech} over one period of the engine's cycle.

$$W_{out} = \int_0^t P_{mech}(t)dt \quad (19)$$

From the simulation results given in Figure 10 the produced mechanical work over one period is equal to W_{out}. The values are summarised in Table 3. The injected enthalpy for one complete intervention (pull and push) is only depending on the volumes of the cylinder and on the pressure. It is identic for the three different lever arms.

Due to the asymmetry of the volumes of the cylinders, the enthalpy injected for one cycle must be calculated in two steps, namely for the filling of the right (a) and left (b) chambers of the first cylinder.

For the enthalpy injected into the chambers two terms remain to be evaluated, namely the internal energy U and the transfer term PΔV.

$$H_{in} = U_a + P_{in} \cdot \Delta V_{1a} + U_b + P_{in} \cdot \Delta V_{1b} \quad (20)$$

Air transfer

$$P_1 \cdot V_{1a} = 4 \cdot 10^5 N/m^2 \cdot 4.24 \cdot 10^{-6} m^3 = 1.696 J \quad (21)$$

$$P_1 \cdot V_{1b} = 4 \cdot 10^5 N/m^2 \cdot 5.65 \cdot 10^{-6} m^3 = 2.26 J \quad (22)$$

The volumes of the right and left chambers have been calculated in rel. 3 and 4.

Internal energies

The internal energies U_a and U_b of the injected compressed air are calculated as

$$U_a = P_1 \cdot V_{1a}(\ln\frac{P_1}{P_a} - 1 + \frac{P_a}{P_1}) = 1.696 J(0.636) = 1.079 J \quad (23)$$

$$U_b = P_1 \cdot V_{1b}(\ln\frac{P_1}{P_a} - 1 + \frac{P_a}{P_1}) = 2.26 J(0.636) = 1.43 J \quad (24)$$

They correspond to an isothermal expansion from a pressure P_1 to an atmospheric environment (Ref. [1]).

ISSN No. 2278-2540 | DOI: 10.51583/IJLTEMAS | Volume XV Issue XI November 2026

The efficiency is calculated over a period of 360° and takes into account the number of interventions of the actuator.

For the 75 mm lever-arm system, there are three right-to-the-left and three left-to-the right motions of the piston assembly and the efficiency becomes

$$\eta = \frac{W_{out}}{3\cdot(P_1\cdot V_{1b} + U_b + P_1\cdot V_{1a} + U_a)} = \frac{12.64J}{3\cdot(1.69J + 1.079J + 2.26J + 1.43J)} = \frac{12.64J}{19.38J} = 0.652$$

For the 50mm lever-arm system, the efficiency is identic (W_{out}=12.63 and same enthalpy).

For the 35mm lever-arm system the value of W_{out} obtained form the simulation is 4.20J, and the enthalpy corresponds to only one push and one pull of the actuator. The efficiency becomes

$$\eta = \frac{W_{out}}{(P_1\cdot V_{1b} + U_b + P_1\cdot V_{1a} + U_a)} = \frac{4.20J}{(1.69J + 1.079J + 2.26J + 1.43J)} = \frac{4.20J}{6.46J} = 0.650$$

r	W_{out}	H_{in}	h
75mm	12.64J	19.38	0.652
50mm	12.63J	19.38	0.652
35mm	4.20J	6.46	0.650

Table 3 Efficiencies of the different engines

Experimental Set-Up

Figure 11 shows the realized experimental set-up with the original cylinder assembly and the control valves (left). At the right side of the picture the coupling mechanism can be seen.

On the front side of the engine shaft the flywheel disc is mounted, and at the rear side the angular position sensor is visible which is realised with a rotating piece with sectors made of electromagnetic material and a proximity sensor.

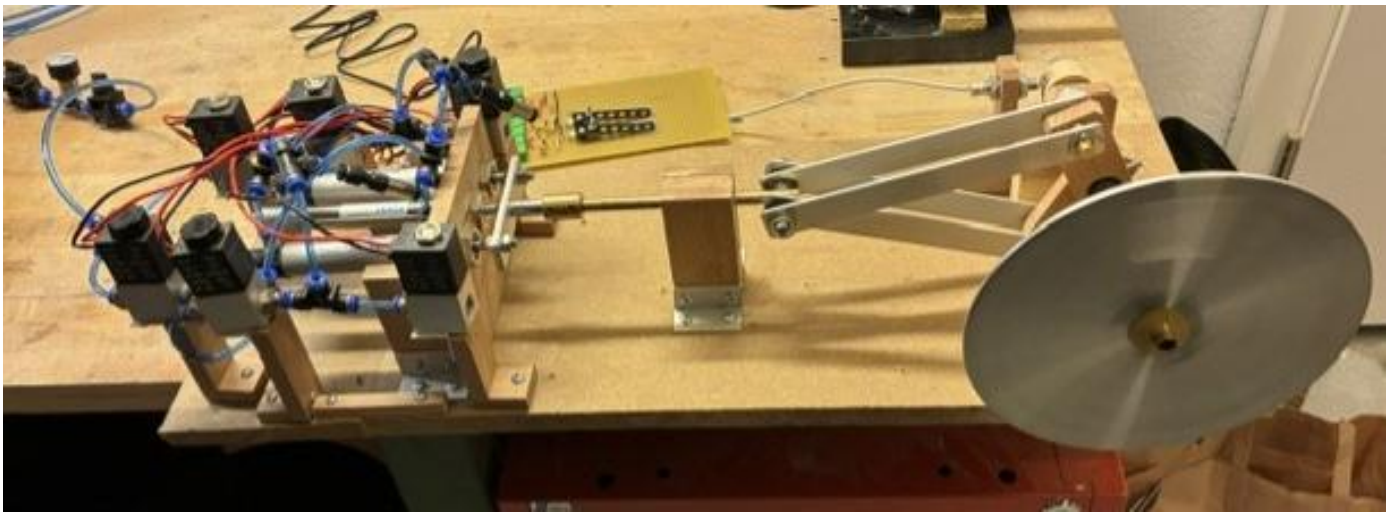


Figure 11 Experimental set-up

ISSN No. 2278-2540 | DOI: 10.51583/IJLTEMAS | Volume XV Issue XI November 2026

Measurements on the experimental set-up

Figure 12 shows the values of the measured pressures during a filling stroke (constant pressure) in the central cylinder followed by an expansion into the two lateral cylinders. This measurement shows a specific effect of the existing dead volumes in the path of air transfer between cylinders, due to tubing and valves. When the central cylinder is filled at a pressure P_1, the expansion phenomenon begins not at that value, but at a pressure P_1'. The change from P_1 to P_1' is due to the transfer of air into the dead volume, causing a pre-expansion [11]. This effect is particularly marked for a system with small cylinders, what is the case of the realized demonstrator.

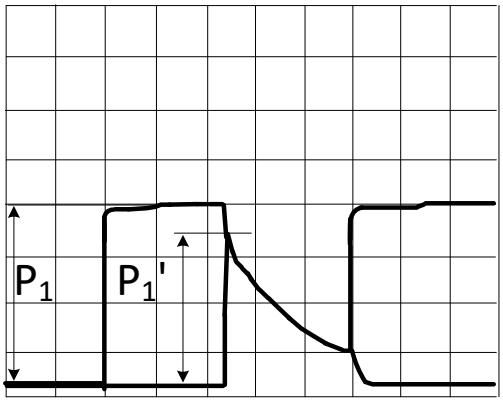


Figure 12 Pressure in the cylinders during filling and expansion ($1*10^5$ N/m^2 per division).

Additionally, the friction of the pistons in the cylinders would be a second source of deviation from the theorical values in terms of efficiency. Especially for small cylinders, when the friction force of the piston is proportional to the diameter and the pressure force proportional to the square of the diameter.

Under these conditions, any measurement of torque, power and mechanical work cannot be used for a practical verification of the simulated performances. Such measurements should be made for a demonstrator of larger dimensions.

The realized small demonstrator could however be considered as a good proof of concept.

CONCLUSIONS

A new compressed air engine has been presented and analysed. The forces developed by a dedicated cylinder assembly have been established by simulation, as also the torque transmitted to the engine's shaft. Produced power and mechanical work, together with the injected enthalpy have allowed to calculate the energetic performance of the motor. The obtained good energy efficiency is the result of the concept of combining constant pressure displacement work with real thermodynamic expansion energy inside of the cylinder assembly.

A comparison of the efficiency obtained with previously investigated systems (ref. 8-11) show that similar values are obtained with the new concept. The relatively high value of around 0.65 is mainly due to the addition of an expansion process of the injected air. The coupling mechanism plays only a minor role, because of all elements of the coupling are not affected by significant losses. These losses can be evaluated as a small part only of the added expansion energy.

The use of double effect single rod pneumatic cylinders has the disadvantage of presenting different pressure areas at the push and pull sides of the pistons in the cylinders, leading to asymmetries as well in the linear forces as in the produced torque of the engine.

ISSN No. 2278-2540 | DOI: 10.51583/IJLTEMAS | Volume XV Issue XI November 2026

In this study the effect of variation of the length of the lever-arms has been investigated. The multiple interventions of the pneumatic actuator within one period has also allowed to increase the average power and as a consequence the converted energy or in other words the produced mechanical work.

The operating principle of the cylinder assembly and of the original coupling mechanism have been verified with a small experimental set-up.

REFERENCES

1. Rufer, A., Energy Storage-Systems and Components, CRC Press, Taylor & Francis group, Boca Raton FL, November, 2017.
2. F. Crotogino, K.-U. Mohmeyer, R. Scharf, Huntorf CAES: More than 20 Years of Successful Operation, Spring 2001 Meeting Orlando Florida USA 15-18 April 2001
3. A.J. Giramonti, R.D. Lessard, W.A. Blecher, E.B. Smith, Conceptual design of compressed air energy storage electric power systems, Appl Energy, vol. 4 (4) pp. 231-249 1978.
4. R. Saidur, N. A. Rahim, M. Hasanuzzaman, A review on compressed-air energy use and energy savings, Renewable and Sustainable Energy Reviews, vol. 14, 4, pp. 1135–1153, 2010.
5. Devang Marvania, Sudhakar Subudhi, A comprehensive review on compressed air powered engine, Renewable and Sustainable Energy Reviews, Volume 70, 2017, Pages 1119-1130, ISSN 1364-0321, https://doi.org/10.1016/j.rser.2016.12.016. (https://www.sciencedirect.com/science/article/pii/S1364032116310681).
6. Atlas Copco, Pocket guide to air motors, 9833 9067 01 2015:1 Jetlag/Boardwalk. Printed in Sweden. © Atlas Copco Industrial Technique AB.
7. Dhumal, A., Ambhore, N., Naik, A. et al. Design and Optimization of Air Motor with Gear Rotor System for Enhanced Performance. J. Inst. Eng. India Ser. C 106, 367–376 (2025). https://doi.org/10.1007/s40032-024-01157-6.
8. Rufer, A., A High Efficiency Pneumatic Drive System Using Vane-Type Semi-Rotary Actuators, Facta Universitatis, Series: Electronics and Energetics Vol. 34, No 3, September 2021, pp. 415-433, https://doi.org/10.2298/FUEE2103415R.
9. Rufer, A., A High Efficiency Pneumatic Motor Based on Double-Acting Linear Cylinders, World Wide Journal of Multidisciplinary Research and Development, WWJMRD, 2021, 7(1), 25-36.
10. Rufer, A., A four-cylinder pneumatic expansion motor with high efficiency, Academia Green Energy, 2(2), April 2025, DOI: 10.20935/AcadEnergy7625.
11. A. Rufer, Semi-Rotary and Linear Actuators for Compressed Air Energy Storage and Energy Efficient Pneumatic Applications, Bentham Science Publishers Pte, Ltd, Singapore, 2023, ISBN 978-981-5179-11-8.
12. H. Liu, Y. Chen, G.L. Tao, G.Z. Jia, W.H. Ding, Research on the displacement and stroke-bore ratio of the air-powered engine, Proceedings of the Sixth International Conference on Fluid Power Transmission and Control (2005), pp. 381-384
13. Yidong Fang, Yiji Lu, Anthony Paul Roskilly, Xiaoli Yu, A review of compressed air energy systems in vehicle transport, Energy Strategy Reviews, Volume 33, 2021, 100583, ISSN 2211-467X,
14. Truglia, Vito Gianfranco, High efficiency engine driven by pressurized air or other compressible gases, US Patent, US 9,677.400 B2 Jun. 13, 2017.
15. Nègre, Guy, Engine with an active mono-energy and/or bi-energy chamber with compressed air and/or additional energy and thermodynamic cycle thereof, US Patent, US 7.469,527 B2, Dec. 30, 2008
16. Koruku, S., Samtas, G., Soy, G., Design and Experimental Investigation of Pneumatic Movement Mechanism Supported by Mechanic Cam and Crank Shaft, TEM Journal, Volume 4 / Number 1 / 2015, www.temjournal.com.
17. FESTO, Fluidic muscle, https://ftp.festo.com/Public/PNEUMATIC/SOFTWARE_SERVICE/Documentation/2020/DE/DMSP-MAS_DE.PDF.
18. Rufer, A., A New Compressed Air Engine Based on Pneumatic Artificial Muscles (PAM's) , Worldwide Journal of Multidisciplinary Research and Development, WWJMRD, 2026, 12(05), pp 14-20.

ISSN No. 2278-2540 | DOI: 10.51583/IJLTEMAS | Volume XV Issue XI November 2026

19. A. Rufer, Clutch Bearing Coupled PAM's (Pneumatic Artificial Muscle) for a Compressed Air Engine, WWJMRD, Worldwide Journal of Multidisciplinary Research and Development, February 2026.
20. Freewheels – Their functions and applications, https://hard-met.pl/wp-content/uploads/2019/06/Freewheel-Clutch.pdf, accessed April 18th 2026.
21. Rufer, A. Deformation Work Recovery for a Compressed Air Engine Driven by Pneumatic Artificial Muscles, Facta Universitatis, Series Electronics and Energetics, Vol. xx, No y 2026, pp pp
22. Rufer, A. Linear Pneumatic Cylinder Assembly with Reduced Air Consumption, October 2023 DOI: 10.2174/978981517909512301000 7 In book: Semi-rotary and Linear Actuators for Compressed Air Energy Storage and Energy Efficient Pneumatic Applications.
23. Rufer, A. Pneumatic Expansion Engine with Freewheeling Clutch Coupling, International Journal of Latest Technology in Engineering Management & Applied Science, 15(9):552-564, October 2026 DOI: 10.51583/IJLTEMAS.2026.150900043.